Characterizing the weathering induced degradation of Poly(ethylene-terephthalate) using PARAFAC modeling of fluorescence spectra

Devin A. Gordon [a], Zhonghao Zhan [b], Laura S. Bruckman [b], *

[a] Department of Macromolecular Science and Engineering, Case Western Reserve University, Cleveland, OH, United States
[b] SDLE Research Center, Department of Materials Science and Engineering, Case Western Reserve University, Cleveland, OH, United States

A B S T R A C T

Poly(ethylene-terephthalate) (PET) film is widely used in photovoltaic module backsheets, for its dielectric breakdown strength, and in applications requiring high optical clarity. PET degrades under exposure to ultraviolet (UV) irradiance, heat, and moisture, which leads to loss of optical clarity and performance properties. To study the weathering driven degradation of PET films, three grades of PET, including unstabilized and stabilized grades, were exposed to three types of accelerated weathering exposure. Fluorescence excitation-emission matrix (EEM) spectra were collected after predetermined exposure intervals. Parallel factor analysis (PARAFAC) was applied to the resulting spectra to decompose the fluorescence data into individual fluorophore components and monitor their relative concentrations over time. EEM-PARAFAC was used to identify and distinguish between the formation of monohydroxy-terephthalate and dihydroxy-terephthalate units in PET over time under the UV-light bearing accelerated exposures. The relative concentrations of these fluorophores were found to increase, while the relative concentration of the PARAFAC component assigned to PET was found to generally decrease. ATR-FTIR was used to support findings from EEM-PARAFAC. Results were also used to assess the impact of additives (UV stabilizer and TiO$_2$) on degradation.

© 2019 Elsevier Ltd. All rights reserved.

1. Introduction

Understanding the degradation of polymeric materials is necessary to predict their lifetimes in applications that demand long term stability. Poly(ethylene-terephthalate) (PET) is a core component of backsheets used as electrical and environmental barriers in photovoltaic (PV) systems. PET is subject to degradation by environmental stressors, such as ultraviolet (UV) light, heat, and humidity, which are described by the Norrish degradation, thermolytic, and hydrolytic degradation mechanisms [1,2]. PET loses its valuable end use properties, such as mechanical strength and dielectric properties, during the degradation process. Fluorescence spectroscopy is highly sensitive to chemical changes in PET during photo-oxidative and thermo-oxidative degradation, and the technique is non-destructive and thus can be used to monitor change over time [1,3].

Previous degradation studies utilizing PET fluorescence have focused on studying the emission or excitation behavior of PET films at single wavelengths in attempt to identify the fluorophore(s) produced by degradation of PET [1,2,4—6]. This paper presents excitation-emission matrix (EEM) spectra that include the full three-dimensional fluorescence spectra of degradation components, which is an improvement from single excitation or emission measurements. This study also applies parallel factor analysis (PARAFAC) to EEM spectra to identify degradation component(s) and extract information on their relative concentrations, yielding quantitative conclusions from spectral analysis instead of qualitative.

PARAFAC is a multi-way modeling technique that decomposes tri-linear data arrays and quantifies the independent underlying signals [7,8]. In previous studies, PARAFAC was applied across a variety of fields from psychometrics to chemometrics primarily as a tool for data interpretation [8—12]. In the analysis of aquatic dissolved organic matter (DOM), scientists characterized the concentrations of aqueous organic species in natural environments by collecting a large number of EEM spectra and fit them to a

previously validated PARAFAC model [13]. This study also confirmed that PARAFAC models are able to be shared throughout the scientific community and can provide insights across multiple studies. Applied to PET degradation studies, PARAFAC facilitates the identification of unique fluorescent groups and aids in the interpretation of and information extraction from higher order data (e.g., EEM fluorescence data). The primary advantage of PARAFAC is that it provides estimates of the excitation and emission spectra and relative concentration profiles of the fluorescence component(s).

The overall aim of this study is to characterize the degradation of PET using EEM fluorescence spectra and apply PARAFAC to gain insights from the data. The paper describes the application of the PARAFAC method and demonstrates the utility of PARAFAC in understanding the impact of weathering stressors and material additives on degradation through interpretation of model results. The paper also seeks to find agreement between PARAFAC results and the literature on PET degradation.

2. Methods

2.1. Materials

Three grades of PET film were examined in this study, denoted as PET, PET-UVS, and PET-TiO$_2$. Both PET and PET-UVS are clear grades of film. PET-UVS contains Tinuvin 360 UV stabilizer. PET-TiO$_2$ is a slightly TiO$_2$-loaded film. Table 1 summarizes some of the properties of the PET films. Films were obtained from commercial sources.

2.2. Study protocol: structure and exposures

A randomized, longitudinal study design was used to study the degradation of PET films. Seven replicates, or identical film samples cut from a large sheet, of each grade of PET film were assigned to three types of accelerated exposures for analysis via fluorescence spectroscopy. (Table 2).

PET films were exposed to ASTM G154 Cycle 4 (G154) and a modified version of ASTM G154 Cycle 4 (mG154) without the dark, condensation cycle for 168 h (one week) step-wise intervals in a QLab QUV Accelerated Weathering Tester [14]. Modified-ASTM G-154 Cycle 4 applied light exposure at 1.5 times the rate of ASTM G154 Cycle 4 due to exclusion of the dark, condensation cycle. The QLab QUV Accelerated Weathering Tester administered light exposure via a UVA-340 fluorescent ultraviolet lamp. Films were also exposed to standard damp heat (DH) conditions (85% relative humidity and 85 °C) for 336 h (two week) step-wise intervals.

A second set of samples composed of one replicate of each grade of PET were exposed to ASTM G154 Cycle 4 and the modified version of ASTM G154 Cycle 4 for analysis via ATR-FTIR. The exposure intervals for the second set of samples were varied.

2.3. Fluorescence spectroscopy

Fluorescence spectroscopy was used to evaluate the degradation of the films after each interval of accelerated exposure. Emission

spectra were collected from 300 nm to 800 nm with 2 nm resolution at excitation wavelengths from 280 nm to 780 nm with increments of 5 nm. The excitation and emission slit widths were 10 nm. Three-dimensional excitation-emission matrix (EEM) plots were generated for each exposure step to observe changes in the fluorescence behavior of the material over time.

2.4. Spectral pre-processing and parallel factor analysis

Pre-processing of the spectra was conducted in RStudio using the eemR package [15]. Corrections were applied to remove first and second order Rayleigh scattering from the EEM spectra. Negative fluorescence intensity values were set to zero.

The EEM spectra were organized in a three-dimensional data array that consisted of: 189 spectra/samples × 251 emission wavelengths × 101 excitation wavelengths. PARAFAC was conducted in RStudio using the multiway package [16]. PARAFAC decomposes the data array into a tri-linear model, which is described by Equation (1).

$$x_{ijk} = \sum_{n=1}^{N} a_{in} b_{jn} c_{kn} + e_{ijk} \qquad (1)$$
$$i = 1, ..., I; j = 1, ..., J; k = 1, ..., K$$

In this study, x_{ijk} is the fluorescence intensity of the kth sample at the ith emission wavelength and the jth excitation wavelength, a_{in} represents the estimated emission spectrum of the nth component, b_{jn} represents the estimated excitation spectrum of the nth component, and c_{kn} is the score or relative concentration of the nth component in sample k. e_{ijk} represents the residuals or error terms of the model. N defines the number of components fit by the model. This technique separates the mixture of fluorescence signals from various compounds without assumptions about the shape of their spectra [7]. The assumption of PARAFAC is that the underlying excitation and emission spectra of the components are different.

The number of PARAFAC components is pre-defined by the user. The optimal number of components was validated using the Bro and Kiers core consistency diagnostic to prevent over-fitting [17]. A non-negativity constraint was applied to each dimension (excitation, emission, and sample) to prevent non-physical results. Components identified by PARAFAC were assigned to chemical species by comparing the resulting excitation and emission spectra to those in literature.

2.5. ATR-FTIR spectroscopy

ATR-FTIR spectroscopy was used to evaluate chemical change of the films as they degraded. Spectra were collected from 650 cm^{-1} to 4000 cm^{-1} with 1 cm^{-1} resolution. Three spectra were collected at each time interval for the second set of samples exposed to ASTM G154 Cycle 4 and Modified-ASTM G154 Cycle 4 to support findings from PARAFAC modeling. Plots of absorbance versus exposure time were generated to observe changes in bonding of the PET structure over time.

2.6. Degraded surface removal

A single unstabilized PET film sample was studied to evaluate the ability of moisture to remove degraded material from the surface of the film. The sample was placed in 50 mL of DI water for 20 min at 60°C following three weeks (504 h) of exposure to Modified-ASTM G154 Cycle 4. The sample was removed from the DI water and the fluorescence spectrum of the resulting solution was measured in aim to detect a fluorescence signal analogous to that of degraded PET.

Table 1
Properties of clear grades of PET film. "Unstabilized" indicates that the samples are free of chemical stabilizers. PVC is the pigment volume concentration of TiO$_2$.

Type	Stabilizer [mol%]	Thickness [μm]	PVC
PET	Unstabilized	254	0
PET-UVS	0.20% Tinuvin 360	127	0
PET-TiO$_2$	Unstabilized	127	0.2

Table 2
Summary of accelerated exposure conditions. T is the black panel temperature for mG154 and G154 and the chamber temperature for DH.

Exposure	Light Segment			
	$UVA_{<360}$ [W/m^2]	T [°C]	Relative Humidity [%]	Duration [hr]
Modified-ASTM G-154 Cycle 4 (mG154)	61	70	Uncontrolled	24
ASTM G-154 Cycle 4 (G154)	61	70	Uncontrolled	8
Damp Heat (DH)	N/A	N/A	N/A	N/A
Exposure	**Dark + Condensation Segment**			
	$UVA_{<360}$ [W/m^2]	T [°C]	Relative Humidity [%]	Duration [hr]
Modified-ASTM G-154 Cycle 4 (mG154)	N/A	N/A	N/A	N/A
ASTM G-154 Cycle 4 (G154)	0	50	Uncontrolled	4
Damp Heat (DH)	0	85	85	24

3. Results

3.1. Excitation-emission fluorescence spectra

The temporal evolution of the corrected EEM spectra of each grade of PET film is presented in Figs. 1–3. The left-most column of each figure shows the EEM spectra of the unexposed samples (Step 0). Step 3 corresponds to 504 exposure hours and Step 6 to 1008 exposure hours for mG154 and G154 exposures. Step 3 corresponds to 1008 exposure hours and Step 6 to 2016 exposure hours for DH exposure. The characteristic fluorescence peak for PET with doublet peak excitation at ~320 nm and ~380 nm and emission peak at ~400 nm can be observed for unexposed PET samples. This characteristic peak is difficult to observe in the unexposed samples of PET-UVS (Fig. 2), due to a combination of dampened fluorescence behavior caused by the UV absorber and the intensity color scale. A decrease in the characteristic peak for PET is accompanied by the

formation of a new fluorescence peak. This change can be observed across the top two rows of each figure as time under ASTM G-154 Cycle 4 and Modified-ASTM G-154 Cycle 4 increases. The new fluorescence peak has doublet peak excitation at ~340 nm and ~385 nm and an emission peak at ~460 nm.

The corrected EEM spectra of DI water (a) and DI water containing degraded PET (b) following the degraded surface removal experiment are shown in Fig. 4. DI water shows no fluorescence signal, whereas DI water containing degraded PET shows a fluorescence peak similar to those of degraded PET shown in Figs. 1–3, but with singlet excitation.

3.2. PARAFAC modeling

PARAFAC models with 1–5 components were fit to the 63 EEM spectra collected to study PET degradation. The core consistency diagnostic, which balances model reliability and complexity, was
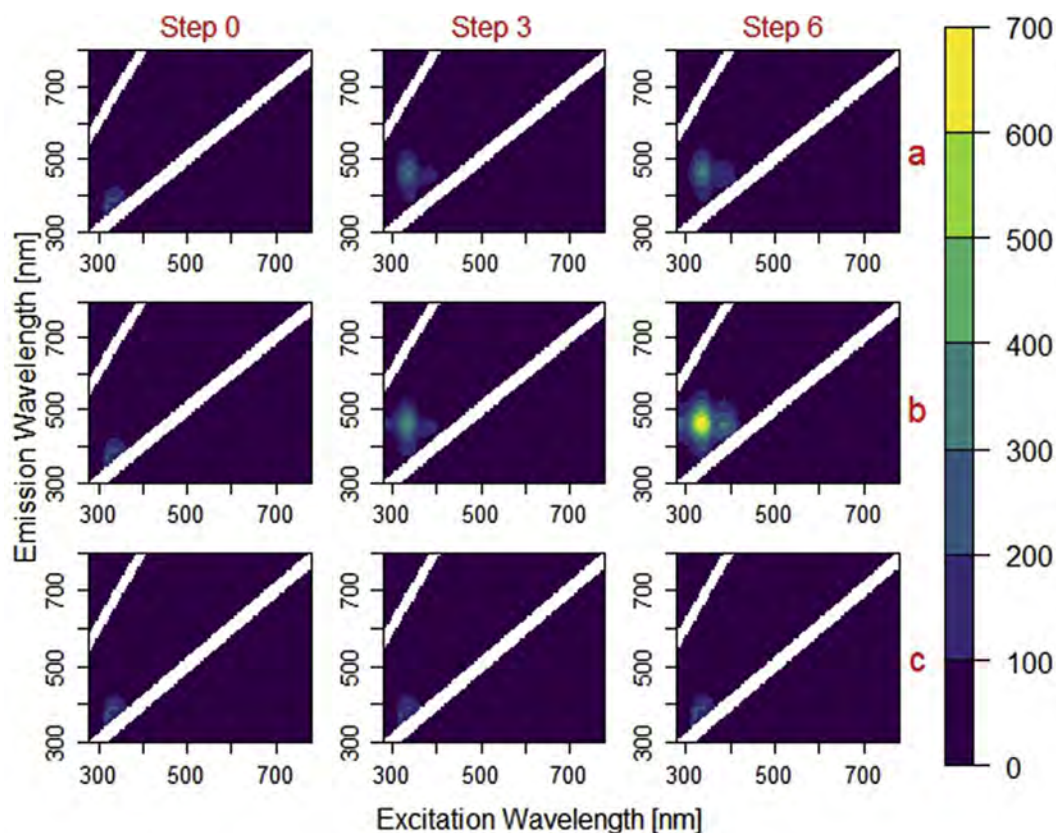

Fig. 1. The temporal evolution of the corrected EEM spectra of PET at three exposure steps. Row "a" corresponds to mG154 exposure, row "b" to G154 exposure, and row "c" to DH exposure.
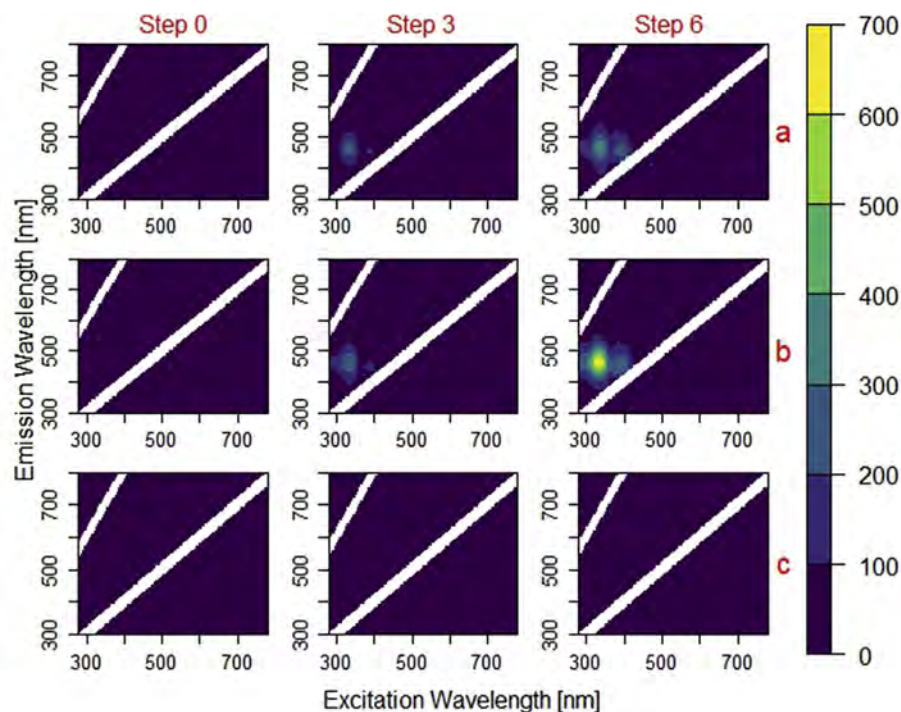
Fig. 2. The temporal evolution of the corrected EEM spectra of PET-UVS at three exposure steps. Row "a" corresponds to mG154 exposure, row "b" to G154 exposure, and row "c" to DH exposure.
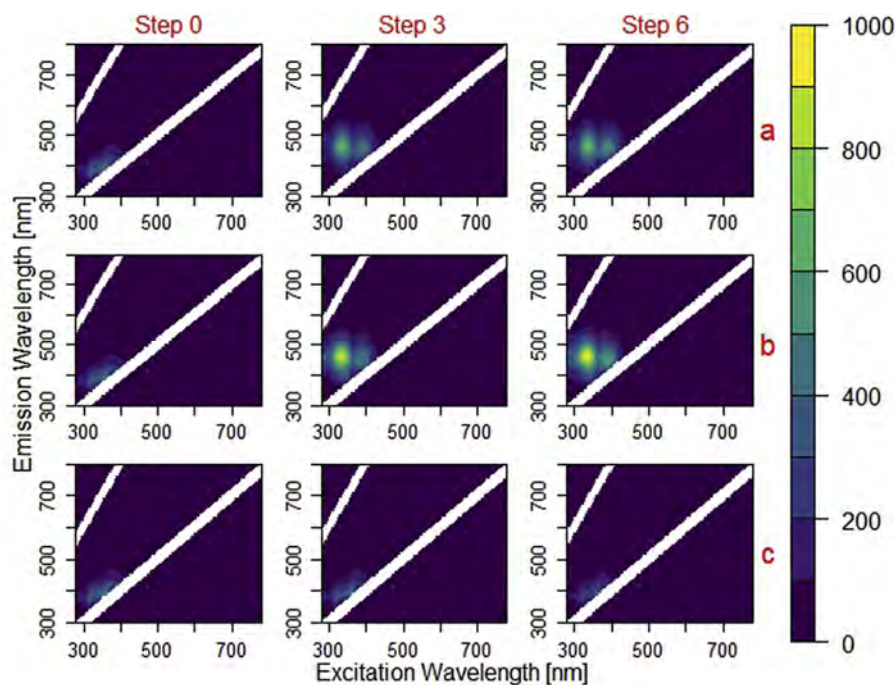

Fig. 3. The temporal evolution of the corrected EEM spectra of PET-TiO$_2$ at three exposure steps. Row "a" corresponds to mG154 exposure, row "b" to G154 exposure, and row "c" to DH exposure.

determined for each model and used to determine the most appropriate number of components. Table 3 shows the resulting core consistency values, a value close to 100% is desirable for model stability, and the diagnostic value sharply decreases when a reliable number of components is exceeded [17].

Three chemical species are expected to contribute to the fluorescent behavior observed in Figs. 1—3 (monohydroxy-terepthalate, dihydroxy-terepthalate, and PET). The three component model has a core consistency value of 1.10%, which indicates that this model may not be stable and hence core consistency points to two
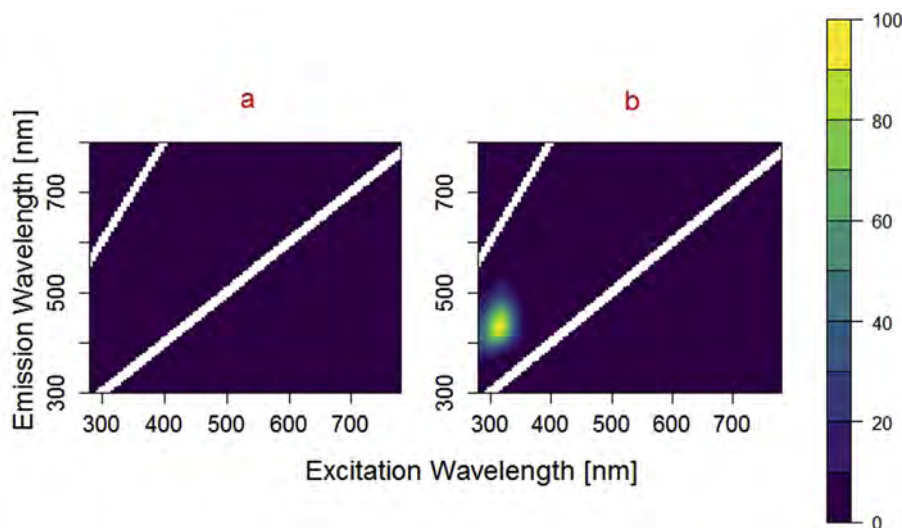
Fig. 4. Corrected EEM fluorescence spectra of DI water ("a") and DI water containing degraded PET ("b") (unstabilized, 504 h of exposure to Modified-ASTM G154 Cycle 4) after the PET film was placed in 50 mL DI water for 20 min at 60°C.

Table 3
Percent explained variance, core consistency values, and number of iterations for PARAFAC models fit with 1–5 components.

	Number of Components				
	1	2	3	4	5
Explained Variance (%)	87.2	93.2	94.9	96.0	96.7
Core Consistency (%)	100	92.9	1.10	−1183	−704
Number of Iterations	4	9	8	13	20

components being optimal. However, the increase percentage of explained variance from a two to three component model points to three components as being a stronger representation of the data.

The same solution is typically obtained for a PARAFAC model if the correct number of components is chosen. When the model is fit with too many components, the number of local minima often increases [7]. The three component model was fit by 100 repeated modeling routines to test its convergence. Three component models with similar component loadings, but with different ordering/permutation of Components 2 and 3, were obtained regardless of the core consistency value, which is not conclusive but indicates that the three component model is a possible solution [13].

Two-factor degeneracy is a situation in which two of the components are virtually identical but have opposite signs, which generally occurs when the model is fit with too many components [7]. In this case, two-factor degeneracy was not found for the three component model. Repeated convergence to the same solution together with the absence of two-factor degeneracy indicate that the three component model is worth consideration. Therefore the three component model was selected for interpretation. This model explained 94.9% of the variability in the data about its mean ($R^2 = 0.949$).

The results of the PARAFAC model, loadings and scores, with three components are presented in Figs. 5–10. The loadings from PARAFAC correspond to the estimated excitation and emission spectra of the responsible fluorescent compound. Fig. 5 shows that Component 1 has fluorescence excitation at ~340 nm and emission centered at ~460 nm. Fig. 6 shows that Component 2 has fluorescence excitation at ~390 nm, peak emission at ~450 nm, and a weak emission band on the right shoulder of the peak. Fig. 7 shows
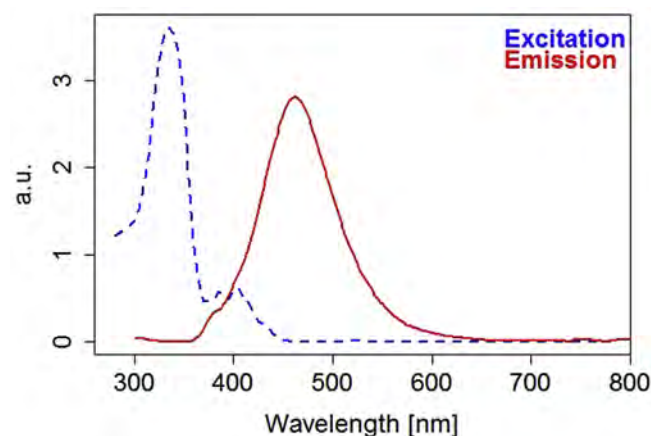

Fig. 5. PARAFAC estimate of the excitation and emission spectra of Component 1. The solid red line corresponds to the emission spectrum and the dashed blue line to the excitation spectrum. Component 1 was assigned to monohydroxy-terepthalate units. (For interpretation of the references to color in this figure legend, the reader is referred to the Web version of this article.)

that Component 3 has fluorescence excitation at ~320 nm and ~360 nm and with peak emission at ~400 nm.

The scores from PARAFAC correspond to the relative concentration of the component in each given EEM spectrum. Scores, relative concentrations, are presented in Figs. 8–10 versus time under exposure. The relative concentrations have been normalized such that components with nonzero initial score (at 0 h of exposure) have unit initial score and to account for differences in fluorescence intensity between materials [18–20]. Normalization allowed comparison between the trends of different materials over time. Figs. 8 and 9 show the increase in relative concentrations of Components 1 and 2 over time in exposures that contained UV light as a stressor. Fig. 10 shows the change in relative concentration of Component 3 over time under exposure.

3.3. ATR-FTIR

FTIR has been widely used to study PET and its oxidative degradation [5,21–25]. The temporal evolution of the ATR-FTIR
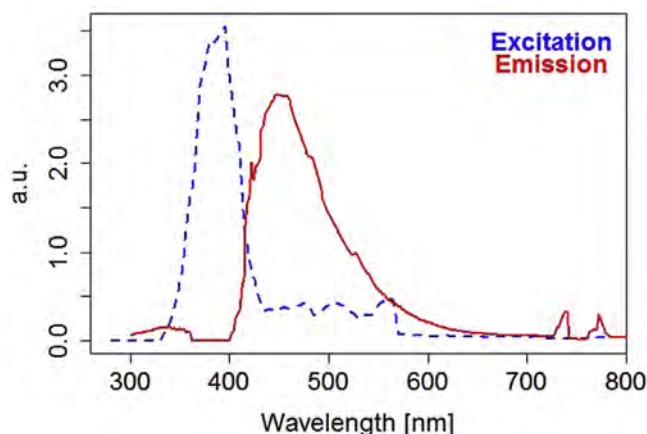
Fig. 6. PARAFAC estimate of the excitation and emission spectra of Component 2. The solid red line corresponds to the emission spectrum and the dashed blue line to the excitation spectrum. Component 2 was assigned to dihydroxy-terephthalate units. (For interpretation of the references to color in this figure legend, the reader is referred to the Web version of this article.)
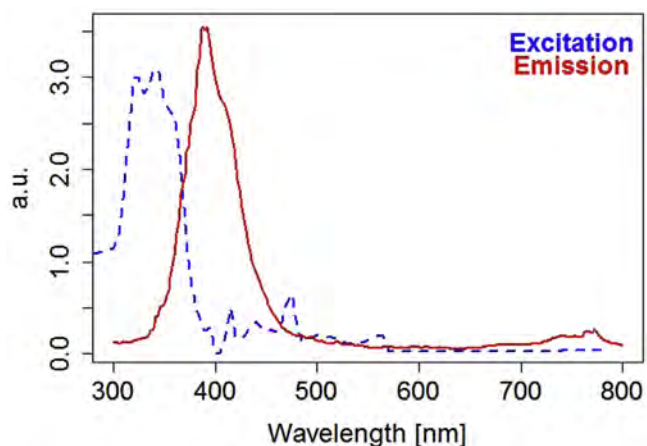

Fig. 7. PARAFAC estimate of the excitation and emission spectra of Component 3. The solid red line corresponds to the emission spectrum and the dashed blue line to the excitation spectrum. Component 3 was assigned to PET. (For interpretation of the references to color in this figure legend, the reader is referred to the Web version of this article.)

spectra of PET under Modified-ASTM G-154 Cycle 4 exposure is shown in Fig. 11 to exemplify spectral changes observed under photolytic degradation. Peaks in the low frequency portion of the fingerprint region of the spectra ($740\,cm^{-1}$ - $900\,cm^{-1}$) are used to assign the substitution pattern about the PET aromatic ring [26]. Figs. 12—14 show the change in absorbance at $780\,cm^{-1}$, $870\,cm^{-1}$, and $880\,cm^{-1}$ over time under ASTM G-154 Cycle 4 and Modified-ASTM G-154 Cycle 4 exposures.

4. Discussion

4.1. Component assignment

The PARAFAC model loadings (Figs. 5—7) were used to assign the components to compounds responsible for the fluorescence behavior. The formation of hydroxy-substituted terephthalate units (monohydroxy-terephthalate and dihydroxy-terephthalate) throughout the PET degradation process has been previously discussed [1,2,4—6]. These products result from the substitution of
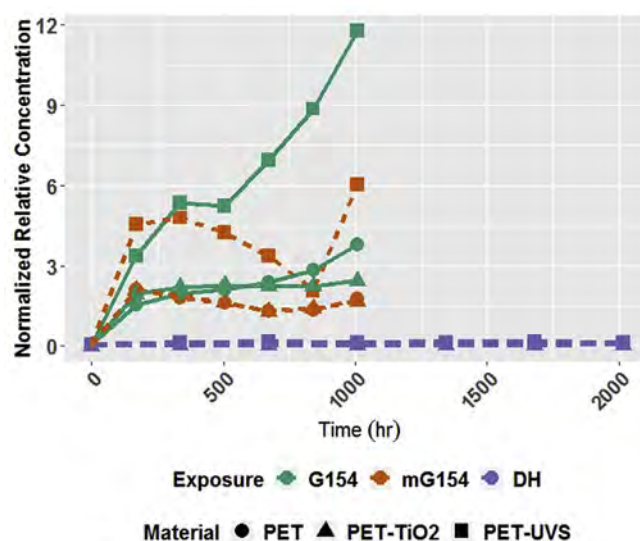

Fig. 8. Normalized relative concentration of Component 1 (monohydroxy-terephthalate units) over time under each exposure for the three grades of PET. Solid green lines correspond to ASTM G-154 Cycle 4 exposure, short-dashed orange lines to Modified-ASTM G-154 Cycle 4 exposure, and long-dashed purple lines to damp heat exposure. Circles correspond to PET, triangles to PET-TiO$_2$, and squares to PET-UVS. (For interpretation of the references to color in this figure legend, the reader is referred to the Web version of this article.)
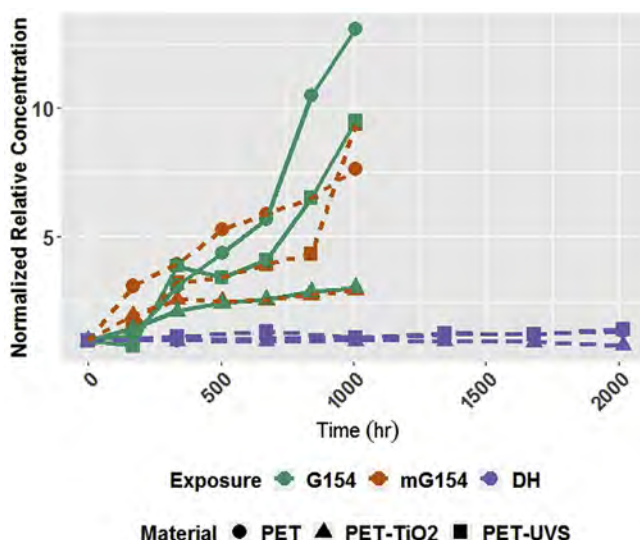

Fig. 9. Normalized relative concentration of Component 2 (dihydroxy-terephthalate units) over time under each exposure for the three grades of PET. Solid green lines correspond to ASTM G-154 Cycle 4 exposure, short-dashed orange lines to Modified-ASTM G-154 Cycle 4 exposure, and long-dashed purple lines to damp heat exposure. Circles correspond to PET, triangles to PET-TiO$_2$, and squares to PET-UVS. (For interpretation of the references to color in this figure legend, the reader is referred to the Web version of this article.)

hydroxyl-radicals, which are generated from the scission of peroxides, onto the aromatic ring [27]. Monohydroxy-terephthalate units are characterized by an excitation peak at $\sim$340 nm and emission at $\sim$460 nm [4,5]. Component 1 was assigned to monohydroxy-terephthalate units, due to its excitation peak at $\sim$340 nm and emission at $\sim$460 nm in its PARAFAC loadings (Fig. 5). Dihydroxy-terephthalate units are characterized by an excitation peak at $\sim$385 nm with emission at $\sim$450 nm and $\sim$520 nm [2,4]. Component 2 was assigned to dihydroxy-terephthalate units, due to
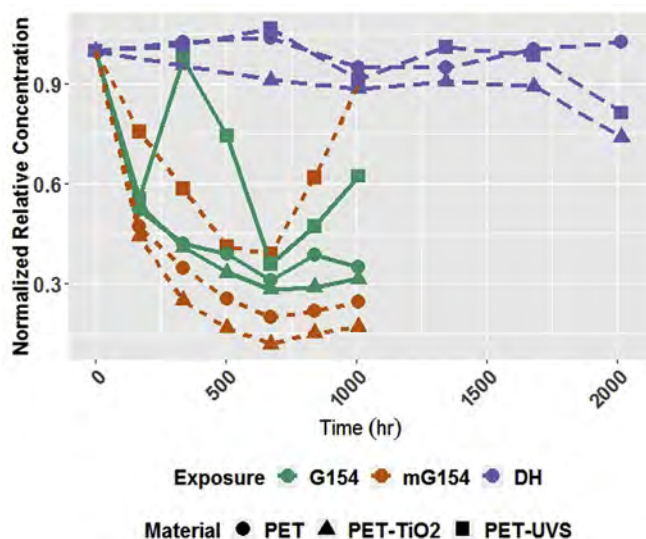
Fig. 10. Normalized relative concentration of Component 3 (PET) over time under each exposure for the three grades of PET. Solid green lines correspond to ASTM G-154 Cycle 4 exposure, short-dashed orange lines to Modified-ASTM G-154 Cycle 4 exposure, and long-dashed purple lines to damp heat exposure. Circles correspond to PET, triangles to PET-TiO₂, and squares to PET-UVS. (For interpretation of the references to color in this figure legend, the reader is referred to the Web version of this article.)

Fig. 12. ATR-FTIR Absorbance at 780 cm⁻¹ versus exposure time under ASTM G-154 Cycle 4 and Modified-ASTM G-154 Cycle 4 for the three grades of PET. Green corresponds to ASTM G-154 Cycle 4 exposure and orange to Modified-ASTM G-154 Cycle 4 exposure. Circles correspond to PET, triangles to PET-TiO₂, and squares to PET-UVS. (For interpretation of the references to color in this figure legend, the reader is referred to the Web version of this article.)
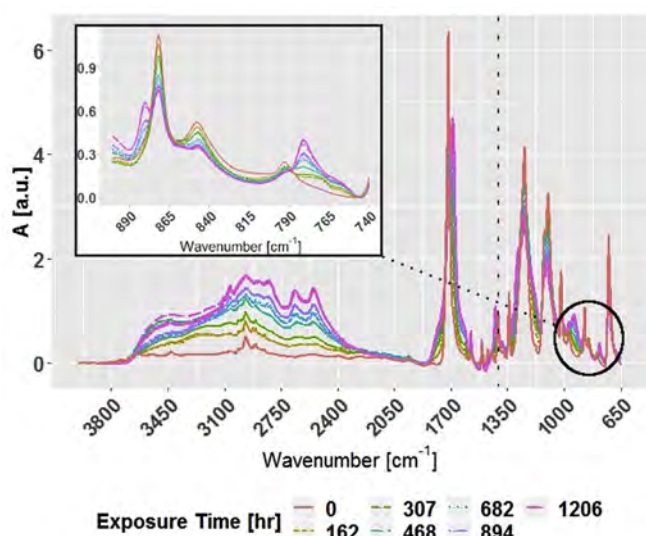

Fig. 11. ATR-FTIR spectra of PET films over time under exposure to Modified-ASTM G154 Cycle 4. The inset spectra highlight the changes in the low frequency portion of the fingerprint region of the spectra (740 cm⁻¹ - 900 cm⁻¹). The vertical dashed line shows the frequency of the peak used for normalization (1410 cm⁻¹).

Fig. 13. ATR-FTIR Absorbance at 870 cm⁻¹ versus exposure time under ASTM G-154 Cycle 4 and Modified-ASTM G-154 Cycle 4 for the three grades of PET. Solid green lines correspond to ASTM G-154 Cycle 4 exposure and short-dashed orange lines to Modified-ASTM G-154 Cycle 4 exposure. Circles correspond to PET, triangles to PET-TiO₂, and squares to PET-UVS. (For interpretation of the references to color in this figure legend, the reader is referred to the Web version of this article.)

its excitation peak at ~390 nm, emission at ~460 nm, and emission shoulder at ~520 nm in its PARAFAC loadings (Fig. 6). Component 3 was assigned to PET because of its characteristic emission peaks at ~390 nm and ~410 nm (Fig. 7) [5].

4.2. Exposure and additive effects

The PARAFAC model scores (Figs. 8–10) were used to assess the impact of exposure conditions and additives on PET degradation. The relative concentrations of Components 2 and 3 were normalized by their initial values (at 0 h) to have unit relative concentration at the beginning of the study. The relative concentrations of
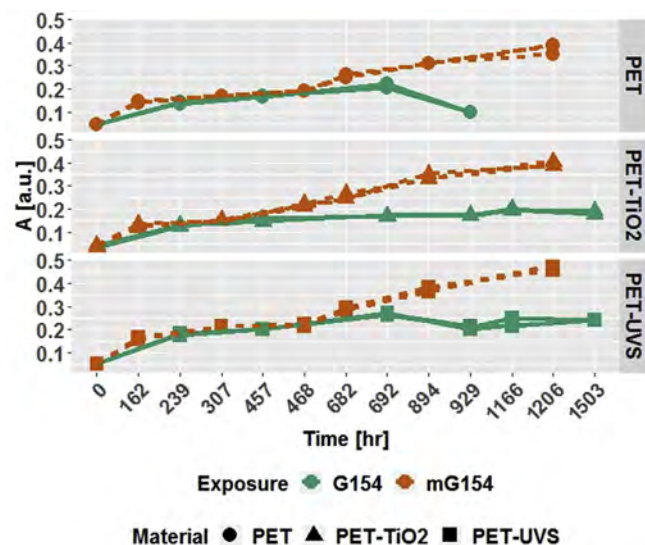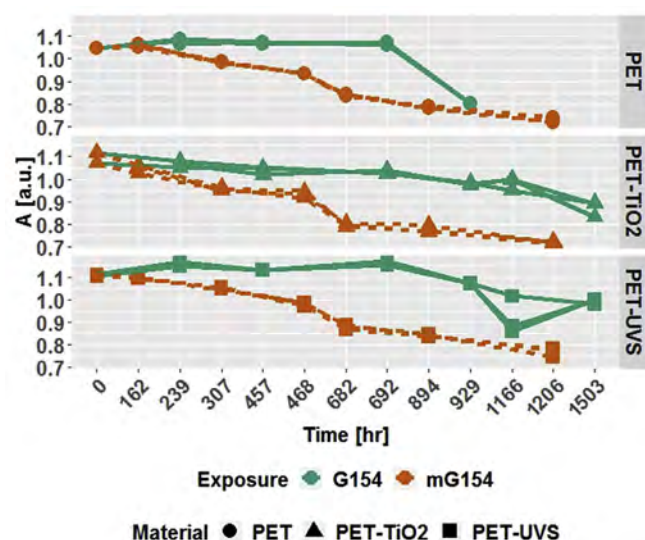
Component 1 were normalized by the initial values of Component 3 to help account for the differences in initial fluorescence intensity of the films.

Figs. 8–10 show that exposure to damp heat conditions did not generate Components 1 nor 2 (mono- and dihydroxy-terephthalate units, respectively), nor did the exposure strongly decrease the relative concentration signal assigned to Component 3 (PET). This finding supports the reaction proposed by Ciolacu et al., as UV light contributes to the generation of hydroxyl radicals that then undergo substitution [27]. Fig. 8 shows that exposure to Modified-
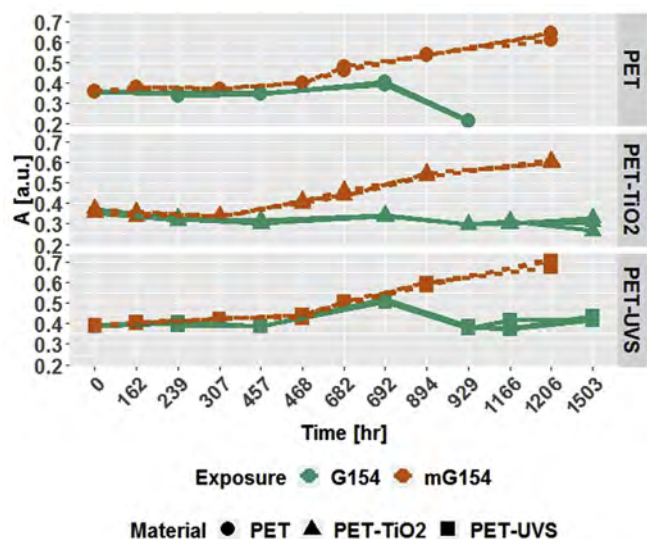
Fig. 14. ATR-FTIR Absorbance at 880 cm^{-1} versus exposure time under ASTM G-154 Cycle 4 and Modified-ASTM G-154 Cycle 4 for the three grades of PET. Green corresponds to ASTM G-154 Cycle 4 exposure and orange to Modified-ASTM G-154 Cycle 4 exposure. Circles correspond to PET, triangles to PET-TiO$_2$, and squares to PET-UVS. (For interpretation of the references to color in this figure legend, the reader is referred to the Web version of this article.)

ASTM G-154 Cycle 4 caused an initial increase in relative concentration of Component 1, followed by a decrease, where as Fig. 9 shows nearly constant increase in the relative concentration of Component 2. These trends provide evidence of the formation of monohydroxy-terephthalate units early in exposure to Modified-ASTM G-154 Cycle 4, followed by their conversion to dihydroxy-terephthalate units as degradation proceeds.

Fig. 8 shows that exposure to ASTM G-154 Cycle 4 did not lead to the decrease of the relative concentration of Component 1 that was observed under exposure to Modified-ASTM G-154 Cycle 4. Given that PET photo-oxidation reactions are concentrated to the surface layers, the formation of monohydroxy-terephthalate units throughout the bulk of the film could be limited once the surface becomes sufficiently degraded under exposure to Modified-ASTM G-154 Cycle 4 [5,28]. In contrast, moisture in the dark, condensation cycle of ASTM G-154 Cycle 4 could have removed degraded material from the surface and allowed further formation of monohydroxy-terephthalate units.

Fig. 4 shows the corrected EEM fluorescence spectra of DI water and DI water containing degraded PET (unstabilized, 504 h of exposure to Modified-ASTM G154 Cycle 4) after the PET film was placed in 50 mL DI water for 20 min at 60°C. Initially the DI water shows no fluorescence signal and following contact with the film the solution shows a fluorescence signal with a peak analogous to the excitation and emission peaks of monohydroxy-terephthalate units (Component 1, Fig. 5). This result shows that moisture can readily remove degraded material from the surface of PET film. Fig. 9 shows that Modified-ASTM G-154 Cycle 4 and ASTM G-154 Cycle 4 formed similar relative concentrations of Component 2 over time, with the exception of unstabilized PET in the late stages of degradation, which supports that the formation of dihydroxy-terephthalate units is governed by conversion from monohydroxy-terephthalate units [27]. Degradation in the PET structure is observed under damp heat conditions as exposure time approached the final 2000 h time step in PET-TiO$_2$ and PET-UVS by a small decrease in relative concentration of Component 3 (Fig. 10).

Figs. 8 and 9 show that PET-TiO$_2$ demonstrated the lowest rate of

formation of Component 1 and Component 2 across both UV exposures. TiO$_2$ can function as a screening compound for PET by absorbing and scattering harmful radiation away from the polymer matrix [29]. PET-UVS appeared to form more of Component 1 than PET. This result is unexpected and is likely complicated by the overall increase in fluorescence of the film as the Tinuvin 360 stabilizer is depleted. Also, PET-UVS generally showed less formation of dihydroxy-terephthalate units (Component 2) than PET, which is likely due to mitigation of initial monohydroxy-substitution by the UV stabilizer.

Fig. 10 shows that the relative concentration of Component 3 decreased for both PET and PET-TiO$_2$ under UV-containing exposures. It also highlights an eventual increase in relative concentration of Component 3 for PET-UVS under UV-bearing exposures, which signifies an increase in the relative intensity of the PET-UVS fluorescence over time. The initial fluorescence of PET-UVS was lower than that of PET (Figs. 2 and 1, respectively), which resulted in a lower unnormalized relative concentration of Component 3 in PET-UVS than in PET. The fluorescence intensity contributing to Component 3 for PET-UVS increased as the Tinuvin 360 degraded with increasing exposure to UV.

The decreased concentration of Tinuvin 360 allowed for stronger excitation and emission phenomena. This behavior explains the increase in relative concentration of Component 3 (assigned to PET) in PET-UVS for the first 336 h of ASTM G-154 Cycle 4 exposure, which is then followed by the decreasing trend that was observed in PET and PET-TiO$_2$. This may also account for the apparent higher relative concentration of Component 1 in PET-UVS than in PET that was observed in Fig. 8. All samples under UV-bearing exposures show increase in the relative concentration of Component 3 (PET) for the final two exposure time steps, which can be attributed to experimental error; the increase is magnified for PET-UVS due to the aforementioned normalization effect.

4.3. Supporting evidence of hydroxy-substitution

ATR-FTIR spectra were used to support conclusions concerning hydroxy-substitution of the PET aromatic ring. Initial increase in absorbance at 780 cm^{-1} and 880 cm^{-1} along with a decrease in peak intensity at 870 cm^{-1} were observed over time under ASTM G-154 Cycle 4 and Modified-ASTM G-154 Cycle 4 exposures (Figs. 12–14). These trends point to changes in the substitution pattern of the PET aromatic ring. The decreasing intensity at 870 cm^{-1} (Fig. 13) is associated with the C-H deformation of two adjacent hydrogens bonded to the aromatic ring, which is indicative loss of the initial para-substitution pattern [26]. The intensities at 780 cm^{-1} and 880 cm^{-1} (Figs. 12 and 14) increase over time as mono- and di-hydroxy-terephthalate form and are associated with the C-H deformation of two lone hydrogens and one lone hydrogen bonded to the aromatic ring, respectively. In addition, increase in peak intensity at 775 cm^{-1} (observed at 780 cm^{-1} in our study) has been reported to be due to photo-oxidation by Scheirs and Gardette, but was not fully assigned [30].

The combination of intensity trends is indicative of a shift from a para-substitution to a 1,2,4-substitution pattern about the aromatic ring, which is in agreement with the substitution pattern of monohydroxy-terephthalate units. Monohydroxy-terephthalate units were expected to be detected at the surface as the polymer is exposed, as opposed to di-hydroxyterephthalate units or PET, by ATR-FTIR because they were present in relatively higher concentrations (Figs. 8–10) and because photodegradation occurs most strongly at the surface [5]. The changes in intensity that indicated shift in substitution pattern were consistent over time under Modified-ASTM G-154 Cycle 4 exposure; however, they reached an apparent steady state after 692 h of exposure under ASTM G-154

Cycle 4 exposure. The observation of apparent steady state behavior under ASTM G-154 Cycle 4 exposure was attributed to removal of material from the surface of the PET films by DI water, which is in agreement with the trend observed for monohydroxy-terephthalate units (Component 1) from the PARAFAC model. Removal of degraded material by moisture caused changes in band intensity to appear slowed or reversed from the perspective of ATR-FTIR, which is only surface-sensitive.

5. Conclusions

Application of PARAFAC to EEM fluorescence spectra has proven useful for characterizing and interpreting the degradation of PET films and examining the underlying roles of exposure stressors and material additives. The three component PARAFAC model yielded excitation and emission spectra that were in agreement with measurements of extracted compounds from previous studies. Formation of hydroxy-substituted terephthalate units only occurred under exposure to UV radiation, in the solid state, and the relative concentration of these units was increased in the presence of moisture. The technique was able to successfully distinguish between the presence of monohydroxy-terephthalate and dihydroxy-terephthalate units and describe their formation over time under exposure. Observation of formation of monohydroxy-terephthalate units by means of fluorescence spectroscopy was supported by findings from ATR-FTIR that suggested the conversion from the initial para-substitution pattern to a 1,2,4-substitution pattern about the PET aromatic ring. Deionized water was found to be capable of removing degraded material from the surface of PET film, which suggests that moisture from condensing humidity prevented the film surface reaching steady state degradation under ASTM G-154 Cycle 4. The Tinuvin 360 UV absorber was found to be temporarily effective in limiting the formation of monohydroxy-terephthalate and its subsequent conversion to dihydroxy-terephthalate and only offered protection during the initial stages of UV exposure. TiO_2 was found to decrease the rate of formation of hydroxy-substituted terephthalate units. Resulting values of relative concentration provide a useful metric for monitoring the degradation of polymeric materials.

Acknowledgment

References

[1] M. Day, D.M. Wiles, Photochemical degradation of poly(ethylene terephthalate). III. Determination of decomposition products and reaction mechanism, J. Appl. Polym. Sci. 16 (1) (1972) 203–215, https://doi.org/10.1002/app.1972.070160118. http://onlinelibrary.wiley.com/doi/10.1002/app.1972.070160118/abstract.

[2] M. Edge, N.S. Allen, R. Wiles, W. McDonald, S.V. Mortlock, Identification of luminescent species contributing to the yellowing of poly(-ethyleneterephthalate) on degradation, Polymer 36 (2) (1995) 227–234, https://doi.org/10.1016/0032-3861(95)91308-T. http://www.sciencedirect.com/science/article/pii/003238619591308T.

[3] J. Yang, Z. Xia, F. Kong, X. Ma, The effect of metal catalyst on the discoloration of poly(ethylene terephthalate) in thermo-oxidative degradation, Polym. Degrad. Stabil. 95 (1) (2010) 53–58, https://doi.org/10.1016/j.polymdegradstab.2009.10.009. http://www.sciencedirect.com/science/article/pii/

S0141391009003346.

[4] J.G. Pacifici, J.M. Straley, Photolysis of terephthalate polyesters: hydroxylation of the aromatic nuclei, J. Polym. Sci. B Polym. Lett. 7 (1) (1969) 7–9, https://doi.org/10.1002/pol.1969.110070102. http://onlinelibrary.wiley.com/doi/10.1002/pol.1969.110070102/abstract.

[5] G. Fechine, M. Rabello, R. Souto Maior, L. Catalani, Surface characterization of photodegraded poly(ethylene terephthalate). the effect of ultraviolet absorbers, Polymer 45 (7) (2004) 2303–2308, https://doi.org/10.1016/j.polymer.2004.02.003. http://www.sciencedirect.com/science/article/pii/S003238610400103X.

[6] T. Grossetîte, A. Rivaton, J.L. Gardette, C.E. Hoyle, M. Ziemer, D.R. Fagerburg, H. Clauberg, Photochemical degradation of poly(ethylene terephthalate)-modified copolymer, Polymer 41 (10) (2000) 3541–3554, https://doi.org/10.1016/S0032-3861(99)00580-7. http://www.sciencedirect.com/science/article/pii/S0032386199005807.

[7] C.M. Andersen, R. Bro, Practical aspects of PARAFAC modeling of fluorescence excitation-emission data, J. Chemometr. 17 (4) (2003) 200–215, https://doi.org/10.1002/cem.790. http://onlinelibrary.wiley.com/doi/10.1002/cem.790/abstract.

[8] K.R. Murphy, C.A. Stedmon, D. Graeber, R. Bro, Fluorescence spectroscopy and multi-way techniques, PARAFAC, Analytical Methods 5 (23) (2013) 6557–6566, https://doi.org/10.1039/C3AY41160E. http://pubs.rsc.org/en/content/articlelanding/2013/ay/c3ay41160e.

[9] J.K. Ford, R.C. MacCALLUM, M. Tait, The application of exploratory factor Analysis in applied psychology: a critical review and analysis, Person. Psychol. 39 (2) (1986) 291–314, https://doi.org/10.1111/j.1744-6570.1986.tb00583.x. https://onlinelibrary.wiley.com/doi/abs/10.1111/j.1744-6570.1986.tb00583.x.

[10] J.C. Hayton, D.G. Allen, V. Scarpello, Factor retention decisions in exploratory factor Analysis: a tutorial on parallel analysis, Organ. Res. Methods 7 (2) (2004) 191–205, https://doi.org/10.1177/1094428104263675. https://doi.org/10.1177/1094428104263675.

[11] N.D. Sidiropoulos, R. Bro, G.B. Giannakis, Parallel factor analysis in sensor array processing, IEEE Trans. Signal Process. 48 (8) (2000) 2377–2388, https://doi.org/10.1109/78.852018.

[12] C.A. Stedmon, R. Bro, Characterizing dissolved organic matter fluorescence with parallel factor analysis: a tutorial, Limnol Oceanogr. Methods 6 (11) (2008) 572–579, https://doi.org/10.4319/lom.2008.6.572. https://aslopubs.onlinelibrary.wiley.com/doi/abs/10.4319/lom.2008.6.572.

[13] J.B. Fellman, M.P. Miller, R.M. Cory, D.V. DAmore, D. White, Characterizing dissolved organic matter using PARAFAC modeling of fluorescence spectroscopy: a comparison of two models, Environ. Sci. Technol. 43 (16) (2009) 6228–6234, https://doi.org/10.1021/es900143g. https://doi.org/10.1021/es900143g.

[14] ASTM G154-16 Standard Practice for Operating Fluorescent Ultraviolet (UV) Lamp Apparatus for Exposure of Nonmetallic Materials, ASTM International, West Conshohocken, PA, 2016. https://doi.org/10.1520/G0154-16.

[15] P. Massicotte, eemR: Tools for Pre-processing Emission-Excitation-Matrix (EEM) Fluorescence Data, R Package Version 0, 2017, .1.5. https://CRAN.R-project.org/package=eemR.

[16] N.E. Helwig, Multiway: Component Models for Multi-Way Data, R Package Version 1, 2017, .0-4. https://CRAN.R-project.org/package=multiway.

[17] R. Bro, H. A. L. Kiers, A new efficient method for determining the number of components in PARAFAC models, J. Chemometr. 17 (5) 274–286. doi:10.1002/cem.801. URL https://onlinelibrary.wiley.com/doi/abs/10.1002/cem.801.

[18] N.L.P. Andrews, J.Z. Fan, R.L. Forward, M.C. Chen, H.-P. Loock, Determination of the thermal, oxidative and photochemical degradation rates of scintillator liquid by fluorescence EEM spectroscopy, Phys. Chem. Chem. Phys. 19 (1) (2016) 73–81, https://doi.org/10.1039/C6CP06015C. https://pubs.rsc.org/en/content/articlelanding/2017/cp/c6cp06015c.

[19] H. Chen, J.E. Kenny, Application of PARAFAC to a two-component system exhibiting Fluorescence Resonance Energy Transfer : from theoretical prediction to experimental validation, Analyst 137 (1) (2012) 153–162, https://doi.org/10.1039/C1AN15805H. https://pubs.rsc.org/en/content/articlelanding/2012/an/c1an15805h.

[20] Jan H. Christensen, Asger B. Hansen, John Mortensen, O. Andersen, Characterization and Matching of Oil Samples Using Fluorescence Spectroscopy and Parallel Factor Analysis, Feb. 2005, https://doi.org/10.1021/ac048213k. https://pubs.acs.org/doi/abs/10.1021/ac048213k.

[21] K. Yoda, A. Tsuboi, M. Wada, R. Yamadera, Network formation in poly(-ethylene terephthalate) by thermooxidative degradation, J. Appl. Polym. Sci. 14 (9) (1970) 2357–2376, https://doi.org/10.1002/app.1970.070140915. http://onlinelibrary.wiley.com/doi/10.1002/app.1970.070140915/abstract.

[22] M. Edge, R. Wiles, N.S. Allen, W.A. McDonald, S.V. Mortlock, Characterisation of the species responsible for yellowing in melt degraded aromatic polyestersI: yellowing of poly(ethylene terephthalate), Polym. Degrad. Stabil. 53 (2) (1996) 141–151, https://doi.org/10.1016/0141-3910(96)00081-X. http://www.sciencedirect.com/science/article/pii/014139109600081X.

[23] I. Donelli, G. Freddi, V.A. Nierstrasz, P. Taddei, Surface structure and properties of poly-(ethylene terephthalate) hydrolyzed by alkali and cutinase, Polym. Degrad. Stabil. 95 (9) (2010) 1542–1550, https://doi.org/10.1016/j.polymdegradstab.2010.06.011. http://www.sciencedirect.com/science/article/pii/S0141391010002478.

[24] C.Y. Liang, S. Krimm, Infrared spectra of high polymers: Part IX. Polyethylene terephthalate, J. Mol. Spectrosc. 3 (1) (1959) 554–574, https://doi.org/10.1016/0022-2852(59)90048-7. http://www.sciencedirect.com/science/

article/pii/0022285259900487.

[25] C. Sammon, J. Yarwood, N. Everall, An FTIR study of the effect of hydrolytic degradation on the structure of thin PET films, Polym. Degrad. Stabil. 67 (1) (2000) 149–158, https://doi.org/10.1016/S0141-3910(99)00104-4. http://www.sciencedirect.com/science/article/pii/S0141391099001044.

[26] B. Holland, J. Hay, The thermal degradation of pet and analogous polyesters measured by thermal analysisfourier transform infrared spectroscopy, Polymer 43 (6) (2002) 1835–1847. https://doi.org/10.1016/S0032-3861(01)00775-3. http://www.sciencedirect.com/science/article/pii/S0032386101007753.

[27] C.F. Ladasiu Ciolacu, N.R. Choudhury, N.K. Dutta, Colour formation in poly(ethylene terephthalate) during melt processing, Polym. Degrad. Stabil. 91 (4) (2006) 875–885, https://doi.org/10.1016/j.polymdegradstab.2005.06.021.

https://www.sciencedirect.com/science/article/pii/S0141391005003046.

[28] G.J.M. Fechine, R.M. Souto-Maior, M.S. Rabello, Photodegradation of multilayer films based on PET copolymers, J. Appl. Polym. Sci. 104 (1) (2007) 51–57, https://doi.org/10.1002/app.24517. http://onlinelibrary.wiley.com/doi/10.1002/app.24517/abstract.

[29] G. Wypych, in: G. Wypych (Ed.), Handbook of Material Weathering (fifth edition), fifth ed. Edition, Elsevier, Oxford, 2013, pp. 49–87. https://doi.org/10.1016/B978-1-895198-62-1.50006-8. http://www.sciencedirect.com/science/article/pii/B9781895198621500068.

[30] J. Scheirs, J.-L. Gardette, Photo-oxidation and photolysis of poly(ethylene naphthalate), Polym. Degrad. Stabil. 56 (3) (1997) 339–350, https://doi.org/10.1016/S0141-3910(96)00199-1. http://www.sciencedirect.com/science/article/pii/S0141391096001991.